Proceedings of the ASME 2015 Dynamic Systems and Control Conference
DSCC 2015
October 28-30, 2015, Columbus, Ohio, USA

DSCC2015-9705

BATTERY CHARGE CONTROL WITH AN ELECTRO-THERMAL-AGING COUPLING

Xiaosong Hu*
Hector E. Perez
Scott J. Moura
Energy, Controls, and Applications Laboratory
Department of Civil and Environmental Engineering
University of California
Berkeley, California 94720
Email: xiaosonghu@berkeley.edu, heperez@berkeley.edu, smoura@berkeley.edu

ABSTRACT

Efficient and safe battery charge control is an important prerequisite for large-scale deployment of clean energy systems. This paper proposes an innovative approach to devising optimally health-conscious fast-safe charge protocols. A multi-objective optimal control problem is mathematically formulated via a coupled electro-thermal-aging battery model, where electrical and aging sub-models depend upon the core temperature captured by a two-state thermal sub-model. The Legendre-Gauss-Radau (LGR) pseudo-spectral method with adaptive multi-mesh-interval collocation is employed to solve the resulting highly nonlinear six-state optimal control problem. Charge time and health degradation are therefore optimally traded off, subject to both electrical and thermal constraints. Minimum-time, minimum-aging, and balanced charge scenarios are examined in detail. The implications of the upper voltage bound, ambient temperature, and cooling convection resistance to the optimization outcome are investigated as well.

1 INTRODUCTION

Batteries are widely utilized in mobile handsets, electric vehicles (EVs), and power grid energy storage [1, 2]. They are an enabling technology for diversifying and securing our future energy supplies. In contrast to simple and rapid refueling of gasoline or diesel, battery recharge requires meticulous control and management, owing to complex electrochemical reactions, immeasurable internal states, and serious safety concerns [3]. Fast charging is a thriving area of research, as it increases the practicality and consumer acceptance of battery-powered devices (e.g., EVs). Nevertheless, it can also impair battery longevity depending on the charging method used, particularly due to heating. It is thus crucial to systematically study the tradeoffs between charging time and health degradation, which is the focus of this paper.

The traditional charging protocol for Li-ion batteries is constant-current/constant-voltage (CCCV) [4]. In the CC stage, the charging current is constant until a pre-specified voltage threshold is reached; in the CV stage the voltage threshold is maintained until the current relaxes below a pre-specified threshold value. This technique is simple and easily implemented. The current rate and voltage threshold are, however, almost universally selected in an ad-hoc manner.

Various methods were proposed to reduce charge times, such as multi-stage CC (high CC followed by low CC) plus CV (MCC-CV) [5], fuzzy logic [6, 7], neural networks [8], grey system theory [9], and ant colony system algorithm [10]. Alternative protocols were reported to prolong the battery lifetime as well, such as MCC-CV (low CC followed by high CC plus CV) [11] and CCCV with negative pulse (CCCV-NP) [12]. These protocols are almost always heuristic. That is, they employ basic knowledge or empirical observations of electrical properties of batteries to devise a charging strategy. Their implementation and performance are subject to cumbersome meta-parameter tun-

*Address all correspondence to this author.

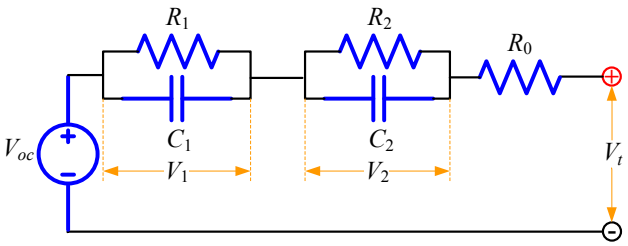

FIGURE 1. SCHEMATIC OF ELECTRICAL MODEL.

ing. Furthermore, there are no mathematical guarantees for fast charge optimality or safe constraint satisfaction.

Recently, some researchers have given first insights into model-based optimal charge control [13–18]. A significant challenge for model-based charge control is numerically solving a multi-state nonlinear calculus of variations optimal control problem. These previous studies side-step this difficulty using linear-quadratic formulations [13], state independent electrical parameters [14], piecewise constant time discretization [15], linear input-output models [16], a one-step model predictive control formulation [17], or a reference governor formulation [18]. To directly face the nonlinear variational calculus problem, orthogonal collocation enabled pseudo-spectral methods were employed in [19] to optimize charging time and efficiency of lithium-ion batteries. However, all of the foregoing studies merely consider the electrical behavior of batteries, without simultaneously accounting for thermal and aging dynamics. Consequently, the optimized protocols may markedly deviate from reality as batteries invariably work at varying thermal and aging conditions. Moreover, aging minimization and temperature-related safety consideration (e.g., overheating avoidance) during charge cannot be explored.

This paper pursues a different approach to developing optimally health-conscious fast-safe charging protocols. Mathematically, we formulate a multi-objective optimal control problem via a coupled electro-thermal-aging model. In the full model, a two-state thermal subsystem captures both core and surface temperature dynamics; and then the core temperature (representing the electrode assembly thermal status) feeds into parameters for the electrical and aging subsystems [20]. Due to the bi-directional coupling between subsystems, the optimization problem is highly nonlinear. Consequently, there are no analytic solutions and numerical solutions have been previously considered intractable. We challenge this entrenched mindset by leveraging the Legendre-Gauss-Radau (LGR) pseudo-spectral method with adaptive multi-mesh-interval collocation. To the best of our knowledge, it is the first multi-objective optimization framework for optimally trading off charging time and battery capacity fade, subject to both electrical and thermal limits. It is also worth highlighting that incorporating a two-state temperature model in lieu of the commonly-used single lumped temperature yields more accurate predictions and safer charging protocols.

The remainder of this paper is structured as follows. In Section 2, the coupled electro-thermal-aging model is described. In Section 3, the multi-objective optimal control problem is formulated, and the LGR pseudo-spectral method is briefly introduced. Optimization results are discussed in Section 4, followed by conclusions in Section 5.

2 COUPLED ELECTRO-THERMAL-AGING MODEL

In this section, a coupled electro-thermal-aging model is described for cylindrical lithium-iron-phosphate batteries (A123 ANR26650M1). It consists of a second-order equivalent circuit model for emulating voltage behavior, a two-state thermal model for predicting the core and surface temperatures, and a semi-empirical capacity-fade model. The electrical parameters depend upon core temperature, SOC, and current direction; the thermal parameters are constant; and the parameters of the aging model depend upon current rate and core temperature. None of the individual subsystem models are new, yet their integration into optimal charging control is novel.

2.1 Electrical Model

The electrical model in Fig. 1 comprises an open-circuit voltage (OCV, V_{oc}), two resistor-capacitor (RC) pairs (R_1, C_1, R_2, C_2), and a resistor (R_0). The state-space model is given by:

$$\frac{dSOC(t)}{dt} = \frac{I(t)}{C_{bat}}, \tag{1}$$

$$\frac{dV_1(t)}{dt} = -\frac{V_1(t)}{R_1C_1} + \frac{I(t)}{C_1}, \tag{2}$$

$$\frac{dV_2(t)}{dt} = -\frac{V_2(t)}{R_2C_2} + \frac{I(t)}{C_2}, \tag{3}$$

$$V_t(t) = V_{oc}(SOC) + V_1(t) + V_2(t) + R_0I(t), \tag{4}$$

where C_{bat} is the nominal capacity, $I(t)$ is the current (positive for charge), and $V_t(t)$ denotes the terminal voltage. The three states include SOC and voltages (V_1, V_2) across the two RC pairs. Through proper experimental design, the electrical parameters have been identified in [20, 21], and those for charge are displayed in Fig. 2.

2.2 Thermal Model

The thermal model sketched in Fig. 3 describes the radial heat transfer dynamics of a cylindrical battery by considering core and surface temperatures T_c and T_s as follows:

$$\frac{dT_c(t)}{dt} = \frac{T_s(t) - T_c(t)}{R_cC_c} + \frac{Q(t)}{C_c}, \tag{5}$$

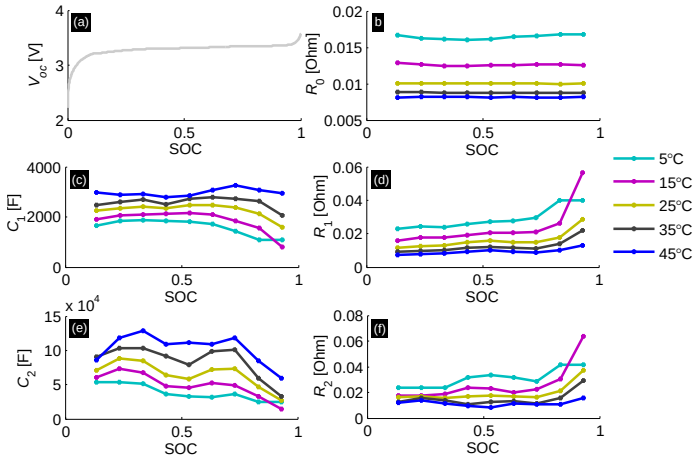

FIGURE 2. ELECTRICAL PARAMETERS FOR CHARGE: (a) V_{oc}, (b) R_0, (c) C_1, (d) R_1, (e) C_2, AND (f) R_2 from [20,21]

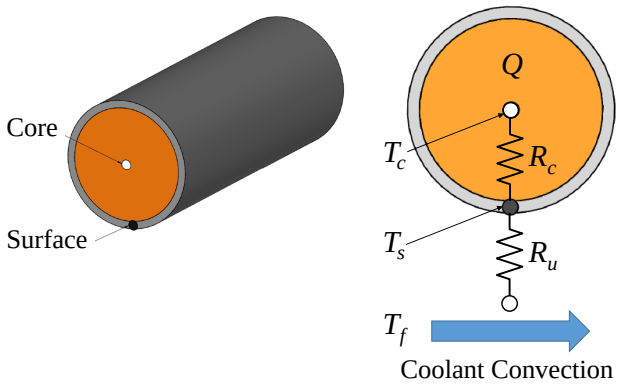

FIGURE 3. SCHEMATIC OF THERMAL MODEL (ADOPTED FROM [20]).

$$\frac{dT_s(t)}{dt} = \frac{T_f(t) - T_s(t)}{R_u C_s} - \frac{T_s(t) - T_c(t)}{R_s C_s}, \tag{6}$$

where $Q(t) = |I(V_{oc} - V_t)|$ is heat generation including joule heating and energy dissipated by electrode over-potentials. The heat conduction resistance, convection resistance, core heat capacity, and surface heat capacity are represented by R_c, R_u, C_c, and C_s, respectively. The two states are the core T_c and surface T_s temperatures. As treated in [20,21], we herein assume that the coolant flow rate is constant, and the ambient temperature T_f is nearly constant. The thermal parameters have been calibrated in previous work and are summarized in Table 1 [20,21].

We remark that the electro-thermal model has been validated over a broad range of loading conditions covering a maximum current rate up to 22C. More details are furnished in [20] regarding the model topology, parameterization, experimental design for identification, and validations.

2.3 Aging Model

We adopt an aging model from [22] that is based upon a matrix of cycling tests. This matrix spans different C-rates[1] (C/2 to 10C), temperatures (-30°C to +60°C), and depths-of-discharge (10% to 90%) for lithium iron phosphate cells (A123 ANR26650M1) in [22]. The experimental data demonstrates that capacity fade depends strongly on C-rate and temperature in these cells, whereas the sensitivity to depth-of-discharge is negligible. A correlation between the capacity loss and the discharged ampere-hour (Ah) throughput has been calibrated by the following semi-empirical model:

$$\Delta Q_b = M(c) \exp\left(\frac{-E_a(c)}{RT_c}\right) A(c)^z, \tag{7}$$

where ΔQ_b is the percentage of capacity loss in [%], c is the C-rate, and $M(c)$ is the pre-exponential factor as a function of the C-rate, (see Table 3 of [22]). Symbol R is the ideal gas constant and A is the discharged Ah throughput depending on C-rate. The activation energy E_a in [J/mol] and the power-law factor z are given by

$$E_a(c) = 31700 - 370.3c, \qquad z = 0.55. \tag{8}$$

A capacity loss of 20% ($\Delta Q_b = 20\%$) is often indicative of the end-of-life (EOL) for an automotive battery, and the corresponding total discharged Ah throughput A_{tol} and number of cycles until EOL, N are algebraically calculated as

$$A_{tol}(c, T_c) = \left[\frac{20}{M(c)\exp\left(\frac{-E_a(c)}{RT_c}\right)}\right]^{\frac{1}{z}}, \tag{9}$$

$$N(c, T_c) = \frac{3600 A_{tol}(c, T_c)}{C_{bat}}, \tag{10}$$

where each cycle corresponds to $2C_{bat}$ charge throughput. Note that A_{tol} is the discharged Ah throughput used by the aging model in [22], and thus the total throughput should be $2A_{tol}$ including both charged and discharged Ah. Based on (9) and (10), the

[1]C-rate is a normalized measure of electric current, defined as the ratio of current $I(t)$ in Amperes, to a cell's nominal capacity C_{bat} in Ampere-hours.

TABLE 1. THERMAL PARAMETERS.

$R_c(K/W)$	$R_u(K/W)$	$C_c(J/K)$	$C_s(J/K)$
1.94	3.19	62.7	4.5

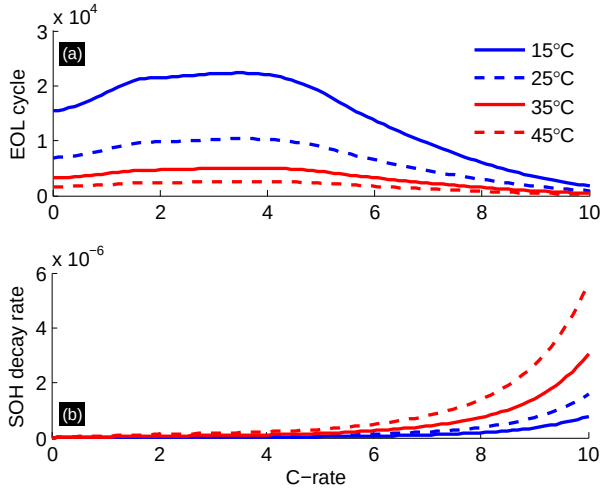

FIGURE 4. BATTERY SOH MODEL: (a) EOL CYCLE $N(c,T_c)$, AND (b) SOH DECAY RATE AS FUNCTIONS OF C-RATE.

battery State-of-Health (SOH) can be defined below:

$$SOH(t) = SOH(t_0) - \frac{\int_{t_0}^{t} |I(\tau)| d\tau}{2N(c,T_c)C_{bat}}, \tag{11}$$

where t_0 denotes the initial time. Consequently, $SOH = 1$ corresponds to a fresh battery and $SOH = 0$ corresponds to 80% capacity loss. The time derivative of (11) yields the dynamical battery aging model

$$\frac{dSOH(t)}{dt} = -\frac{|I(t)|}{2N(c,T_c)C_{bat}}. \tag{12}$$

The EOL cycle number and SOH decay rate, as a function of the C-rate and core temperature, are visualized in Fig. 4. As the C-rate or core temperature increases, the SOH decay rate increases. It is worth pointing out that more EOL cycles can be sustained at medium C-rates (2-5C) than at low C-rates, since the aging model includes calendar-life effects as well (one cycle at a very low C-rate has a dramatically increased duration). The aging model was validated in [22] has been previously applied to component sizing and energy management in hybrid electric vehicles [23, 24].

2.4 Full Model

Combining the above three sub-models produces the coupled electro-thermal-aging model (block diagram in Fig. 5) used for the subsequent charging protocol optimization. The model

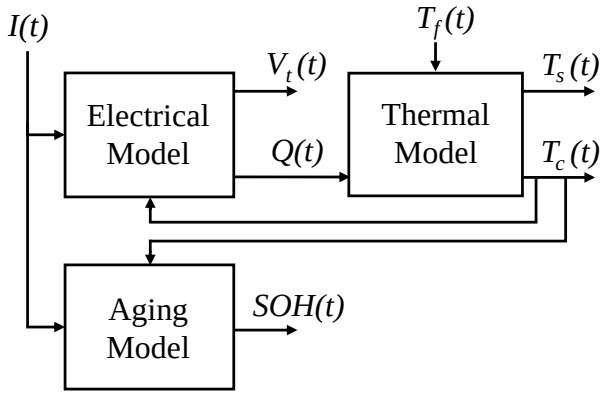

FIGURE 5. ELECTRO-THERMAL-AGING MODEL COUPLING.

dynamics are summarized in (13)-(18), with output equation (4).

$$\frac{dSOC(t)}{dt} = \frac{I(t)}{C_{bat}}, \tag{13}$$

$$\frac{dV_1(t)}{dt} = -\frac{V_1(t)}{R_1C_1} + \frac{I(t)}{C_1}, \tag{14}$$

$$\frac{dV_2(t)}{dt} = -\frac{V_2(t)}{R_2C_2} + \frac{I(t)}{C_2}, \tag{15}$$

$$\frac{dT_c(t)}{dt} = \frac{T_s(t) - T_c(t)}{R_cC_c} + \frac{I(t)(V_1(t) + V_2(t) + R_0I(t))}{C_c}, \tag{16}$$

$$\frac{dT_s(t)}{dt} = \frac{T_f(t) - T_s(t)}{R_uC_s} - \frac{T_s(t) - T_c(t)}{R_sC_s}, \tag{17}$$

$$\frac{dSOH(t)}{dt} = -\frac{|I(t)|}{2N(c,T_c)C_{bat}}. \tag{18}$$

3 FORMULATION OF OPTIMAL CHARGE CONTROL

The objective function J combines charge time with capacity loss (i.e. SOH decay) as follows:

$$\min_{I(t),x(t),t_f} \quad J = \beta \cdot \frac{t_f - t_0}{t_{\max} - t_0} + (1-\beta) \cdot (SOH(t_0) - SOH(t_f)), \tag{19}$$

where t_f is the final time of charge and $0 \le \beta \le 1$ weights the relative importance between the two objectives. The optimization variables are the input current $I(t)$, state variables $x(t) = [SOC(t), V_1(t), V_2(t), T_c(t), T_s(t), SOH(t)]^T$, and final time t_f. The constraints include the model dynamics (13)-(18) and the electrical, thermal, health, and time limits below:

$$SOC_{\min} \le SOC \le SOC_{\max}, \qquad I_{\min} \le I \le I_{\max}, \tag{20}$$

$$SOC(t_0) = SOC_0, \qquad V_{t,\min} \le V_t \le V_{t,\max}, \tag{21}$$

$$SOC(t_f) = SOC_f, \qquad T_{c,\min} \le T_c \le T_{c,\max}, \tag{22}$$

$$SOH_{\min} \le SOH \le SOH_{\max}, \qquad T_c(t_0) = T_{c,0}, T_s(t_0) = T_{s,0}, \tag{23}$$

$$SOH(t_0) = SOH_0, \qquad t_0 \le t \le t_{\max}. \tag{24}$$

Since the optimal control problem has six states and is highly nonlinear, it is difficult to use conventional optimization techniques, e.g., dynamic programming, Pontryagin's minimum principle, and indirect methods, due to intractable computational burden or accuracy. Instead, we pursue pseudo-spectral methods to transcribe this infinite-dimensional optimal control problem into a finite-dimensional optimization problem with algebraic constraints at the discretized nodes. Then, the optimization variables at such nodes are solved by off-the-shelf nonlinear programming (NLP) solvers, like SNOPT or IPOPT [25]. Note that convexity is not guaranteed, and therefore these solvers yield locally optimal solutions. Pseudo-spectral methods are an effective tool for complex nonlinear optimal control problems and have been extensively applied to real-world optimization problems in engineering, including aerospace and autonomous flight systems [26], road vehicle systems [27], energy storage [19], etc. There are a myriad of approaches for discretizing integral and differential equations, leading to a spectrum of pseudo-spectral variants. In this study, we use the Legendre-Gauss-Radau (LGR) pseudo-spectral method with adaptive multi-mesh-interval collocation, featured by the general purpose optimal control software (GPOPS-II) [25]. This software incorporates an orthogonal collocation method to generate the LGR points. Rather than a traditional fixed global mesh, an adaptive mesh refinement algorithm is employed to iteratively adjust the number of mesh intervals, the width of each interval, and the polynomial degree (the number of LGR points). More theoretical and algorithmic properties of this method and GPOPS-II are elaborated in [28, 29] and in the Appendix.

4 RESULTS AND DISCUSSION

This section presents optimization results for three illustrative charge paradigms: minimum-time charge, minimum-aging charge, and balanced charge. The physical bounds in (20)-(24) and ambient temperature T_f are specified as follows:

$$SOC_{\min} = SOC_0 = 0.2, \qquad SOC_{\max} = SOC_f = 0.9, \tag{25}$$
$$I_{\min} = 0A = 0C, \qquad I_{\max} = 46A = 20C, \tag{26}$$
$$V_{t,\min} = 2V, \qquad V_{t,\max} = 3.6V, \tag{27}$$
$$T_{c,\min} = 5^\circ C, \qquad T_{c,\max} = 45^\circ C, \tag{28}$$
$$T_{c,0} = T_{f,0} = 25^\circ C, \qquad T_f(t) = 25^\circ C \ \ \forall t \ge t_0, \tag{29}$$
$$SOH_{\min} = 0, \qquad SOH_{\max} = SOH_0 = 1, \tag{30}$$
$$t_0 = 0sec, \qquad t_{\max} = 36000sec. \tag{31}$$

Here, the voltage limits are selected according to the manufacturer's specification sheet, and the temperature and current limits are chosen based on the validated range in [20].

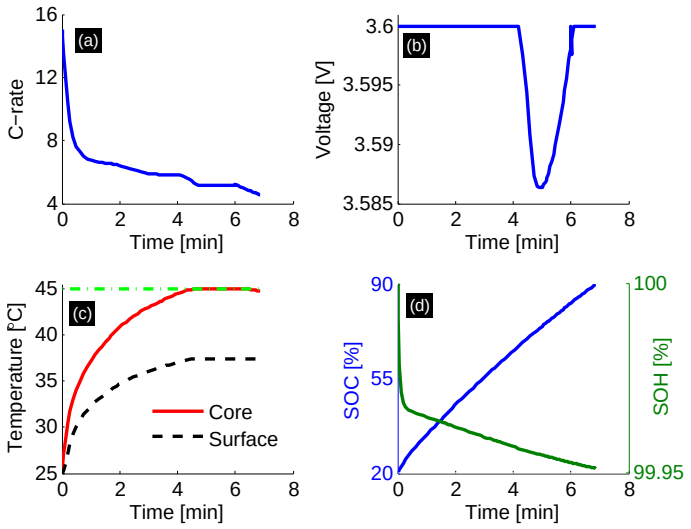

FIGURE 6. OPTIMIZATION RESULT FOR MINIMUM TIME CHARGE: (a) C-RATE, (b) TERMINAL VOLTAGE, (c) CORE AND SURFACE TEMPERATURES, AND (d) SOC/SOH.

4.1 Minimum-Time Charge

By setting $\beta = 1$, the optimization produces a minimum-time charge protocol. The optimal trajectories are shown in Fig. 6. It takes 6.86 minutes to achieve the target SOC. Heuristically, the charge process follows a constant-voltage/constant-temperature (CVCT) protocol. To minimize charging time, the maximum C-rate is applied initially, causing the maximum voltage constraint to become active. The core temperature increases until it reaches its maximum value, which becomes the dominant inequality constraint. This induces a momentary voltage drop.

A comparison is made with CCCV charges with varying C-rates (see Fig. 7). It is clear that CCCV are sub-optimal and/or infeasible. Despite a shorter charge time of 6.76 min, CCCV with 15C violates the maximum temperature constraint $T_c(t) \le T_{c,\max} = 45^\circ C$. CCCV with 10C yields a 6.91 min charge time and trajectory that is very similar to the optimal solution. In other words, this analysis yields the insight that CCCV with 10C happens to be nearly-optimal in the sense of minimizing charge time.

4.2 Minimum-Aging Charge

By setting $\beta = 0$, we can investigate the other extreme – a minimum aging charge protocol. The optimization result is illustrated in Fig. 8. Interestingly, the protocol is pulse-like, while maintaining relatively low core temperature. The resulting SOH decay is approximately 0.004%, more than one order of magnitude less than the SOC decay from minimum-time charging (SOH decay of approximately 0.05%). As shown in Fig. 9, a

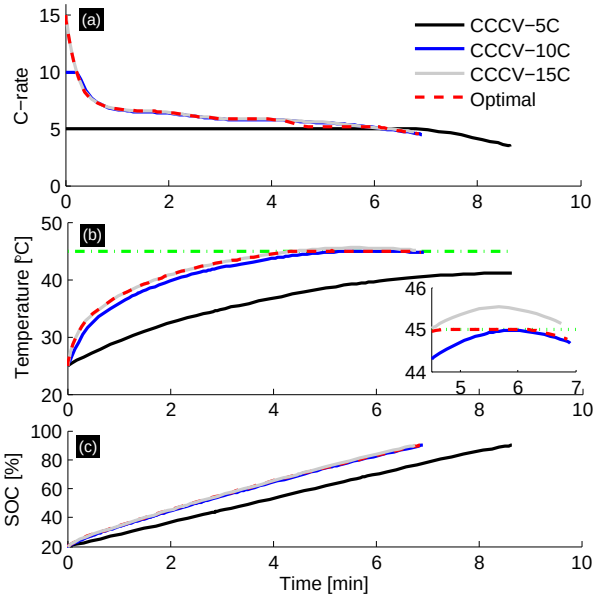

FIGURE 7. COMPARISON WITH CCCV CHARGE: (a) C-RATE, AND (b) CORE TEMPERATURE.

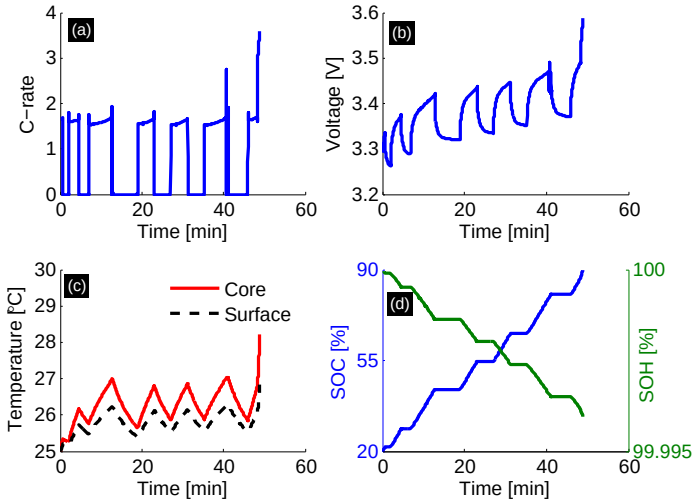

FIGURE 8. OPTIMIZATION RESULT FOR MINIMUM-AGING CHARGE: (a) C-RATE, (b) TERMINAL VOLTAGE, (c) CORE AND SURFACE TEMPERATURES, AND (d) SOC/SOH.

comparison is performed with a C/10 constant-current charge that is widely perceived as a minimum-aging choice. Under the models considered here, the relatively slow C/10 constant-current charge is in fact non-optimal, since the long duration significantly contributes to calendar-life decay.

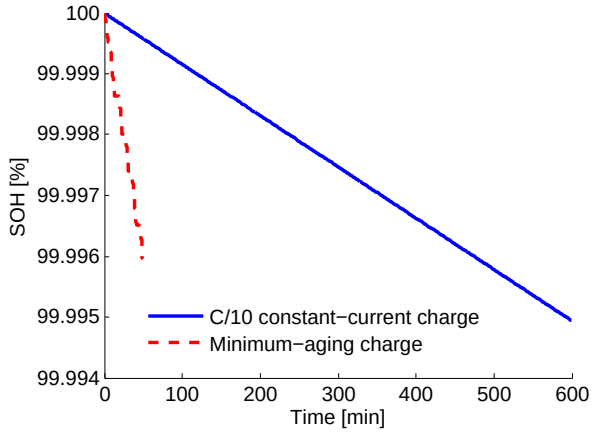

FIGURE 9. SOH TRAJECTORIES OF MINIMUM-AGING CHARGE AND 10-HOUR CONSTANT CURRENT-CHARGE.

4.3 Balanced Charge

By sweeping β values between 0 and 1, we compute a Pareto frontier of balanced charge protocols, i.e., the optimal tradeoffs between fast charge time and SOH decay displayed in Fig. 10. Not surprisingly, the two objectives conflict. Consider the region between the left two data labels in Fig. 10. Battery SOH decay can be substantially mitigated with a negligible increase in charge time. Therefore, one may sacrifice a trivial amount of fast charge time to circumvent rapid SOH decay.

A "balanced" protocol ($\beta = 0.05$) is exemplified in Fig. 11, which can be interpreted as the smallest-aging solution in the case of 12.22-minute charge duration. Note the highly non-intuitive nature of this charging protocol. The current is carefully regulated to limit the increase of core temperature (a dominant accelerating factor of capacity fade). That is, the current reduces in the first 6 minutes to slow down the temperature rise. Next, current increases in the vicinity of the smallest resistance (see Fig. 12); and ultimately the current diminishes with the enlarged resistance at high *SOC*. The optimal solution exploits nonlinear model properties to improve charge time and SOH decay.

4.4 Sensitivity of Pareto Curve

Next we example solution sensitivity to perturbations in the constraint parameters.

4.4.1 Upper Voltage Bound $V_{t,\max}$ The impact of the upper voltage bound $V_{t,\max}$ on the Pareto curve is shown in Fig. 13 (Top). As $V_{t,\max}$ decreases, the Pareto curve moves to the upper-right and shrinks, resulting in reduced control flexibility. Diminishing $V_{t,\max}$ is therefore unfavorable to both control objectives (charge time reduction and SOH decay mitigation). For example, compared to $V_{t,\max} = 3.6V$, the minimum charge time increases by about 39.1% and 106.8% in the cases of $V_{t,\max} = 3.55V$ and $V_{t,\max} = 3.5V$, respectively.

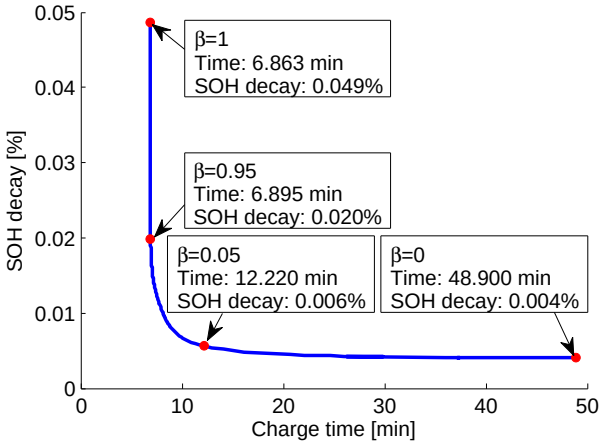

FIGURE 10. PARETO CURVE, CHARGE TIME VS. SOH DECAY.

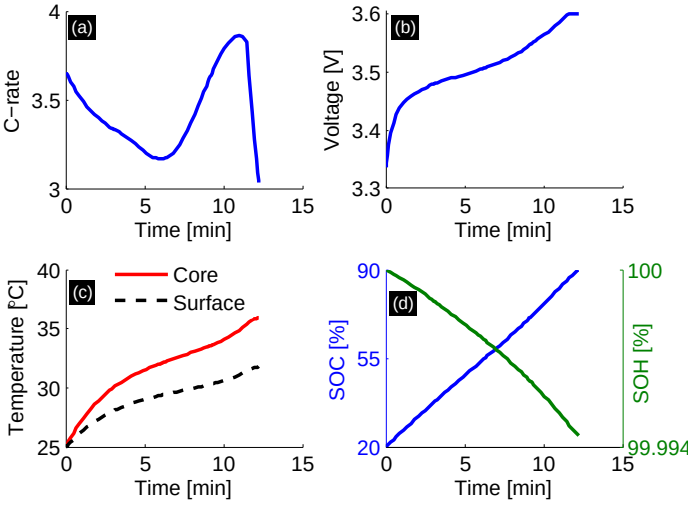

FIGURE 11. OPTIMIZATION RESULT FOR BALANCED CHARGE ($\beta = 0.05$): (a) C-RATE, (b) TERMINAL VOLTAGE, (c) CORE & SURFACE TEMPERATURES, AND (d) SOC/SOH.

4.4.2 Ambient Temperature T_f The impact of the ambient temperature T_f is shown in Fig. 13 (Middle). At low ambient temperature ($T_f = 10°C$), the battery SOH decays slower, whereas the minimum charge time increases due to greater internal resistance. That is, the maximum voltage is reached sooner, because of higher ohmic overpotential. At high ambient temperature ($T_f = 35°C$), the battery SOH decays faster, and the minimum charge time increases because the maximum core temperature is reached sooner, compared to the ambient temperature.

4.4.3 Cooling Convection Resistance R_u The impact of cooling convection resistance R_u is shown in Fig. 13 (Bottom). Given a relatively large R_u (e.g., natural convection), the battery SOH decays faster, and the minimum charge time increases because the maximum core temperature is reached sooner. In the case of $R_u = 1.20K/W$(forced convection), the battery SOH decay is alleviated, but the minimum charge time increases because internal resistance increases as the core temperature decreases, compared to the case of $R_u = 3.19K/W$.

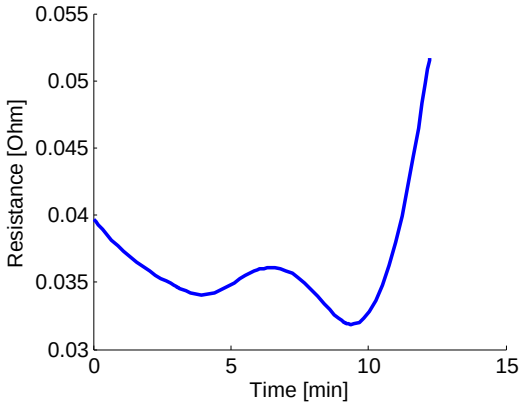

FIGURE 12. TRAJECTORY OF TOTAL EQUIVALENT RESISTANCE ($R_0 + R_1 + R_2$) FOR BALANCED CHARGE ($\beta = 0.05$).

4.5 Further Discussion

The influence of battery aging on the electrical parameters is not addressed in this work, as it has a substantially longer time scale than the SOC and thermal dynamics. While a fresh battery ($SOH_0 = 1$) is herein considered before charge, the proposed optimization framework applies to different aging levels, provided that the associated SOH_0 and electrical parameters are available via recalibration or estimation [30, 31].

5 CONCLUSIONS

A multi-objective optimal control framework has been developed to explore model-based fast-safe charging protocols. In this framework, a coupled electro-thermal-aging model is incorporated to account for thermal constraints and aging effects. The Legendre-Gauss-Radau (LGR) pseudo-spectral method with adaptive multi-mesh-interval collocation is leveraged to solve the infinite dimensional nonlinear optimal control problem. Charge time and battery capacity fade is optimally traded off, subject to both electrical and thermal constraints, a first to the authors' knowledge. Three charging regimes are analyzed in detail, with the following key findings: (i) Minimum-time charge: the protocol is constant-voltage/constant-temperature (CVCT), requiring 6.86 minutes to replenish the SOC from 20% to 90%. (ii) Minimum-aging charge: the protocol is pulse-like rather than a slow constant current charge such as C/10. The associated SOH decay is 0.004%, more than one order of magnitude smaller than that in the minimum-time case. (iii) Balanced charge: the Pareto chart demonstrates that a fundamental tradeoff exists between charge time and SOH decay. A slight (even negligible) time in-

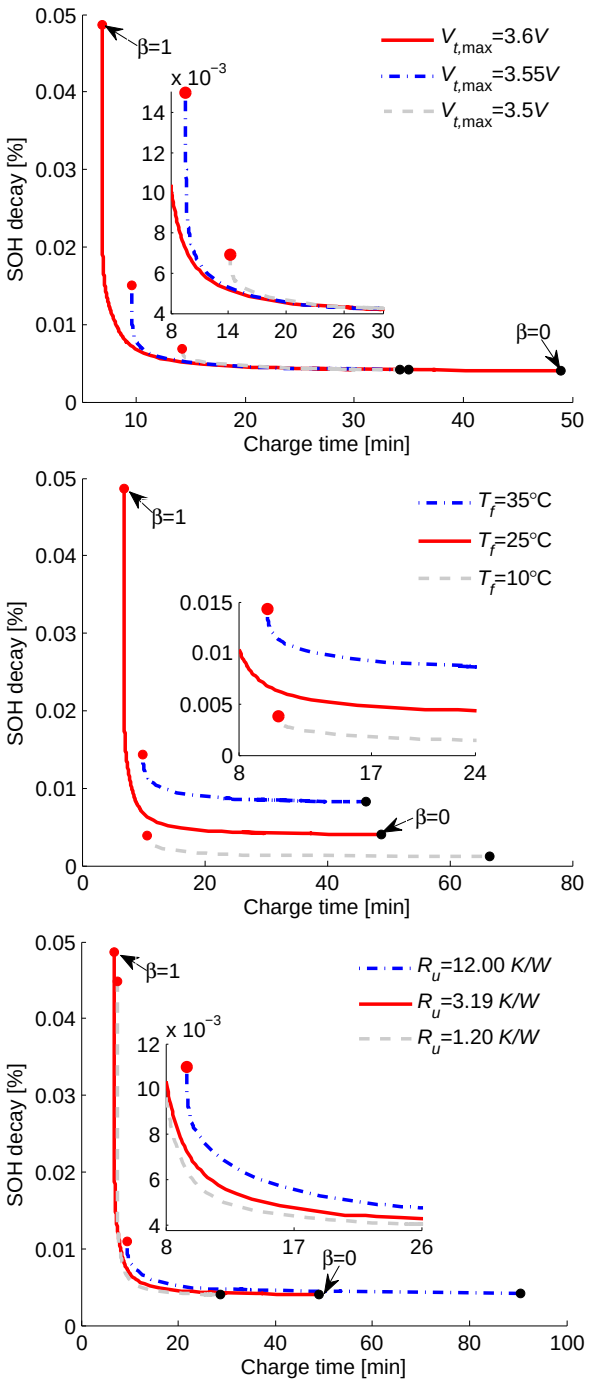

FIGURE 13. TOP: INFLUENCE OF $V_{t,\max}$ ON PARETO CURVE. MIDDLE: INFLUENCE OF T_f ON PARETO CURVE. BOTTOM: INFLUENCE OF R_u ON PARETO CURVE.

crease, relative to the minimum-time case, can significantly alleviate SOH decay. Finally, we examine solution sensitivity to variations in several constraint parameters, including maximum voltage, ambient temperature, and cooling convection resistance.

REFERENCES

[1] Moura, S., Chaturvedi, N., and Krstic, M., 2012. "Pde estimation techniques for advanced battery management systems - part i: Soc estimation". In American Control Conference (ACC), 2012, pp. 559–565.

[2] Hu, X., Murgovski, N., Johannesson, L., and Egardt, B., 2014. "Comparison of three electrochemical energy buffers applied to a hybrid bus powertrain with simultaneous optimal sizing and energy management". *IEEE Trans. on Intelligent Transportation Systems,* ***15***(3), June, pp. 1193–1205.

[3] Yilmaz, M., and Krein, P., 2013. "Review of battery charger topologies, charging power levels, and infrastructure for plug-in electric and hybrid vehicles". *IEEE Trans. on Power Electronics,* ***28***(5), May, pp. 2151–2169.

[4] Zhang, S., Xu, K., and Jow, T., 2006. "Study of the charging process of a licoo2-based li-ion battery". *Journal of Power Sources,* ***160***(2), pp. 1349 – 1354. Special issue including selected papers presented at the International Workshop on Molten Carbonate Fuel Cells and Related Science and Technology 2005 together with regular papers.

[5] Ansean, D., Gonzalez, M., Viera, J., Garcia, V., Blanco, C., and Valledor, M., 2013. "Fast charging technique for high power lithium iron phosphate batteries: A cycle life analysis". *Journal of Power Sources,* ***239***(0), pp. 9 – 15.

[6] Surmann, H., 1996. "Genetic optimization of a fuzzy system for charging batteries". *IEEE Trans. on Industrial Electronics,* ***43***(5), Oct, pp. 541–548.

[7] Liu, Y.-H., and Luo, Y.-F., 2010. "Search for an optimal rapid-charging pattern for li-ion batteries using the taguchi approach". *IEEE Trans. on Industrial Electronics,* ***57***(12), Dec, pp. 3963–3971.

[8] Ullah, Z., Burford, B., and Dillip, S., 1996. "Fast intelligent battery charging: neural-fuzzy approach". *IEEE Aerospace and Electronic Systems Magazine,* ***11***(6), Jun, pp. 26–34.

[9] Chen, L.-R., Hsu, R., and Liu, C.-S., 2008. "A design of a grey-predicted li-ion battery charge system". *IEEE Trans. on Industrial Electronics,* ***55***(10), Oct, pp. 3692–3701.

[10] Liu, Y.-H., Teng, J.-H., and Lin, Y.-C., 2005. "Search for an optimal rapid charging pattern for lithium-ion batteries using ant colony system algorithm". *IEEE Trans. on Industrial Electronics,* ***52***(5), Oct, pp. 1328–1336.

[11] Zhang, S. S., 2006. "The effect of the charging protocol on the cycle life of a li-ion battery". *Journal of Power Sources,* ***161***(2), pp. 1385 – 1391.

[12] Monem, M. A., Trad, K., Omar, N., Hegazy, O., Mantels, B., Mulder, G., den Bossche, P. V., and Mierlo, J. V., 2015. "Lithium-ion batteries: Evaluation study of different charging methodologies based on aging process". *Applied Energy,* ***152***(0), pp. 143 – 155.

[13] Parvini, Y., and Vahidi, A., 2015. "Maximizing Charging Efficiency of Lithium-Ion and Lead-Acid Batteries Using Optimal Control Theory". In 2015 American Control Con-

ference.
[14] Abdollahi, A., Raghunathan, N., Han, X., Avvari, G. V., Balasingam, B., Pattipati, K. R., and Bar-Shalom, Y., 2015. "Battery Charging Optimization for OCV-Resistance Equivalent Circuit Model". In 2015 American Control Conference.
[15] Ravi Methekar, Venkatasailanathan Ramadesigan, R. D. B., and Subramanian, V. R., 2010. "Optimum charging profile for lithium-ion batteries to maximize energy storage and utilization". *ECS Trans.,* ***25***(35), pp. 139–146.
[16] Torchio, M., Wolff, N. A., Raimondo, D. M., Magni, L., Krewer, U., Gopaluni, R. B., Paulson, J. A., and Braatz, R. D., 2015. "Real-time Model Predictive Control for the Optimal Charging of a Lithium-ion Battery". In 2015 American Control Conference.
[17] Klein, R., Chaturvedi, N., Christensen, J., Ahmed, J., Findeisen, R., and Kojic, A., 2011. "Optimal charging strategies in lithium-ion battery". In American Control Conference (ACC), 2011, pp. 382–387.
[18] Perez, H., Shahmohammadhamedani, N., and Moura, S., 2015. "Enhanced performance of li-ion batteries via modified reference governors and electrochemical models". *IEEE/ASME Trans. on Mechatronics,* ***PP***(99), pp. 1–10.
[19] Hu, X., Li, S., Peng, H., and Sun, F., 2013. "Charging time and loss optimization for linmc and lifepo4 batteries based on equivalent circuit models". *Journal of Power Sources,* ***239***(0), pp. 449 – 457.
[20] Lin, X., Perez, H. E., Mohan, S., Siegel, J. B., Stefanopoulou, A. G., Ding, Y., and Castanier, M. P., 2014. "A lumped-parameter electro-thermal model for cylindrical batteries". *Journal of Power Sources,* ***257***(0), pp. 1 – 11.
[21] Perez, H. E., Siegel, J. B., Lin, X., Stefanopoulou, A. G., Ding, Y., and Castanier, M. P., 2012. "Parameterization and validation of an integrated electro-thermal cylindrical lfp battery model". In ASME 2012 5th Annual Dynamic Systems and Control Conference, Dynamic Systems and Control Division, ASME, pp. 41–50.
[22] Wang, J., Liu, P., Hicks-Garner, J., Sherman, E., Soukiazian, S., Verbrugge, M., Tataria, H., Musser, J., and Finamore, P., 2011. "Cycle-life model for graphite-lifepo4 cells". *Journal of Power Sources,* ***196***(8), pp. 3942 – 3948.
[23] Ebbesen, S., Elbert, P., and Guzzella, L., 2012. "Battery state-of-health perceptive energy management for hybrid electric vehicles". *IEEE Trans. on Vehicular Technology,* ***61***(7), Sept, pp. 2893–2900.
[24] Hu, X., Johannesson, L., Murgovski, N., and Egardt, B., 2015. "Longevity-conscious dimensioning and power management of the hybrid energy storage system in a fuel cell hybrid electric bus". *Applied Energy,* ***137***(0), pp. 913 – 924.
[25] Patterson, M. A., and Rao, A. V., 2014. "Gpops-ii: A matlab software for solving multiple-phase optimal control problems using hp-adaptive gaussian quadrature collocation methods and sparse nonlinear programming". *ACM Trans. on Mathematical Software (TOMS),* ***41***(1).
[26] Ross, I. M., and Karpenko, M., 2012. "A review of pseudospectral optimal control: From theory to flight". *Annual Reviews in Control,* ***36***(2), pp. 182 – 197.
[27] Limebeer, D., Perantoni, G., and Rao, A., 2014. "Optimal control of formula one car energy recovery systems". *International Journal of Control,* ***87***(10), pp. 2065–2080.
[28] Darby, C. L., Hager, W. W., and Rao, A. V., 2011. "An hp-adaptive pseudospectral method for solving optimal control problems". *Optimal Control Applications and Methods,* ***32***(4), pp. 476–502.
[29] Garg, D., Hager, W. W., and Rao, A. V., 2011. "Pseudospectral methods for solving infinite-horizon optimal control problems". *Automatica,* ***47***(4), pp. 829 – 837.
[30] Moura, S. J., Chaturvedi, N. A., and Krstic, M., 2014. "Adaptive Partial Differential Equation Observer for Battery State-of-Charge/State-of-Health Estimation Via an Electrochemical Model". *ASME Journal of Dynamic Systems, Measurement, and Control,* ***136***(1), pp. 011015–011015–11.
[31] Hu, X., Li, S. E., Jia, Z., and Egardt, B., 2014. "Enhanced sample entropy-based health management of li-ion battery for electrified vehicles". *Energy,* ***64***(0), pp. 953 – 960.
[32] Garg, D., Patterson, M., Francolin, C., Darby, C., Huntington, G., Hager, W., and Rao, A., 2011. "Direct trajectory optimization and costate estimation of a finite-horizon and infinite-horizon optimal control problems using a radau pseudospectral method". *Computational Optimization and Applications,* ***49***(2), pp. 335–358.
[33] Garg, D., Patterson, M., Hager, W. W., Rao, A. V., Benson, D. A., and Huntington, G. T., 2010. "A unified framework for the numerical solution of optimal control problems using pseudospectral methods". *Automatica,* ***46***(11), pp. 1843 – 1851.

Appendix: Pseudo-Spectral Optimal Control

We summarize the LGR pseudo-spectral method for solving optimal control problems [25, 29, 32, 33]. Consider a general optimal control problem formulated in Bolza form,

$$\min_{x(t),u(t),p} \quad J = \phi(t_0, x(t_0), t_f, x(t_f), p) + \int_{t_o}^{t_f} f(t, x(t), u(t), p)dt, \tag{32}$$

$$\text{s. to:} \quad \frac{dx(t)}{dt} - g(t, x(t), u(t), p) = 0, \tag{33}$$

$$l(t, x(t), u(t), p) = 0, \tag{34}$$

$$h(t, x(t), u(t), p) \leq 0, \tag{35}$$

$$l_b(x(t_0), x(t_f), u(t_0), u(t_f), p) = 0, \tag{36}$$

where $t_0 \le t \le t_f$ is the optimization horizon. Variables t_0 and t_f can be fixed or free optimization variables. The vector p contains either fixed parameters, free parameters to be optimized, or both. Obtaining the numerical solution of the optimal control problem involves three steps: (1) the transcription of the optimal control problem into a nonlinear programming problem (NLP); (2) the solution of the (sparse) NLP; and (3) an examination of the solution accuracy, discretization grid refinement, and then repeating these three steps.

The accuracy and efficiency of this numerical process depends on various factors within the three steps, particularly the first step. Before the three steps, the time interval $t_0 \le t \le t_f$ in the original problem is normalized to $-1 \le \tau \le 1$, by the change of variable $t = \frac{t_f - t_0}{2}\tau + \frac{t_f + t_0}{2}$, which yields

$$\min_{x(\tau),u(\tau),p} \quad J = \phi(t_0, x(-1), t_f, x(1), p) + \frac{t_f - t_0}{2}\int_{-1}^{1} f(\tau, x(\tau), u(\tau), p)d\tau, \tag{37}$$

$$\text{s. to:} \quad \frac{dx(t)}{d\tau} - \frac{t_f - t_0}{2} g(\tau, x(\tau), u(\tau), t_0, t_f, p) = 0, \tag{38}$$

$$l(\tau, x(\tau), u(\tau), t_0, t_f, p) = 0, \tag{39}$$

$$h(\tau, x(\tau), u(\tau), t_0, t_f, p) \le 0, \tag{40}$$

$$l_b(x(-1), x(1), u(-1), u(1), t_0, t_f, p) = 0. \tag{41}$$

The discretization principle of LGR pseudo-spectral method is illustrated as follows. The N-th order Legendre polynomial is

$$P_N(\tau) = \frac{1}{2^N N!}\frac{d^N}{d\tau^N}(\tau^2 - 1)^N. \tag{42}$$

The collocation points are the roots of $P_N(\tau) + P_{N-1}(\tau)$, denoted by τ_i for $i = 1, 2, ..., N$, and $\tau_{N+1} = 1$. The Lagrange interpolating polynomial is defined as

$$L_i(\tau) = \prod_{j=1, j\neq i}^{N+1} \frac{\tau - \tau_j}{\tau_i - \tau_j}. \tag{43}$$

Then the state vector is approximated by

$$x(\tau_i) \approx \sum_{j=1}^{N+1} L_j(\tau_i) x(\tau_j), \tag{44}$$

$$\frac{dx(\tau_i)}{d\tau} \approx \sum_{j=1}^{N+1} \frac{dL_j(\tau_i)}{d\tau} x(\tau_j) = \sum_{j=1}^{N+1} D_{i,j}\, x(\tau_j), \tag{45}$$

where $D_{i,j}$ represents the (i, j) element of the difference matrix $D \in \mathbb{R}^{N\times(N+1)}$. The system dynamics (38) are approximated by

$$\sum_{j=1}^{N+1} D_{i,j} x(\tau_j) - \frac{t_f - t_0}{2} g(\tau_i, x(\tau_i), u(\tau_i), t_0, t_f, p) = 0. \tag{46}$$

The integral term in the objective function (37) is approximated by Gaussian quadrature,

$$\int_{-1}^{1} f(\tau, x(\tau), u(\tau), t_0, t_f, p)d\tau \approx \sum_{i=1}^{N} \omega_i f(\tau_i, x(\tau_i), u(\tau_i), t_0, t_f, p), \tag{47}$$

$$\text{where} \qquad \omega_i = \int_{-1}^{1} L_i(\tau)d\tau. \tag{48}$$

The optimal control problem can now be transcribed into the following NLP,

$$\min_{x(\tau_i),u(\tau_i),p,t_f} \quad J = \phi(t_0, x(-1), t_f, x(1), p) + \sum_{i=1}^{N} \omega_i f(\tau_i, x(\tau_i), u(\tau_i), t_0, t_f, p), \tag{49}$$

$$\text{s. to:} \quad \sum_{j=1}^{N+1} D_{i,j} x(\tau_j) - \frac{t_f - t_0}{2} g(\tau_i, x(\tau_i), u(\tau_i), t_0, t_f, p) = 0, \tag{50}$$

$$l(\tau_i, x(\tau_i), u(\tau), t_0, t_f, p) = 0, \tag{51}$$

$$h(\tau_i, x(\tau_i), u(\tau_i), t_0, t_f, p) \le 0, \tag{52}$$

$$l_b(x(-1), x(1), u(-1), u(1), t_0, t_f, p) = 0, \tag{53}$$

which can be efficiently solved by SNOPT or IPOPT (the co-state vector can also be estimated by the KKT conditions of NLP and the co-state mapping theorem [25, 29, 32, 33].)

The multi-mesh-interval collocation segments the optimal control problem first, and then employs the aforementioned orthogonal collocation technique within each segment. GPOPS-II uses a two-tiered (hp) adaptive grid refinement strategy that refines both the integration segmentation (h) and the orthogonal polynomial order (p). If the integration error across a particular segment is uniform, the order of polynomial collocation points may be increased. If the error at an isolated point within the segment is significantly larger than those at other points within the segment, it may be subdivided (at these large-error points). See [25, 33] for additional details.